

# Residual Strength of Cracked Tubular Joint Using Nonlinear Finite Element Analysis



Natarajan Vignesh Chellappan and Seenainaidu Nallayarasu

**Abstract** Fixed offshore platforms have been used for extraction of oil and gas. These platforms were primarily constructed using steel frames made of tubular members welded at joint or specially fabricated joints. The tubular joints are vulnerable to fatigue-induced cracks which initiate at joints and may propagate through its design life. If the platform life is extended depending upon oil and gas availability, the initial cracks may extend beyond acceptable limits. In recent times, the research on evaluation of residual strength of cracked tubular connection has been considerably increasing since the platforms in various oil and gas fields are ageing. To determine the residual capacity of cracked T-tubular joints, a nonlinear finite element analysis has been carried out. The FEM model of uncracked T joint was validated with experimental result available in literature. The benchmark study has also been made on uncracked T-joints with a specific  $d/D$ ,  $t/T$  and  $D/2T$  and compared with the results obtained from empirical equations (API RP 2A). The possible crack locations have been identified using the maximum SCF at crown and saddle points for axial loads. The cracks are introduced in the maximum SCF locations of tubular joint. The study has been extended to range of  $d/D$  and  $D/2T$ . A correlation has been established between lengths of crack to the residual strength for various crack locations investigated. The residual strength obtained has been compared with reduction factor (BS 7910). It was also found that the residual strength of joints decreases with increase in  $D/2T$ .

**Keywords** T-tubular joints · Crack · Residual strength · SCF  
Extended finite element (XFEM) analysis

---

N. Vignesh Chellappan (✉) · S. Nallayarasu  
Department of Ocean Engineering, IIT Madras, 600036 Chennai, India  
e-mail: [goglemail2vicky@gmail.com](mailto:goglemail2vicky@gmail.com)

© Springer Nature Singapore Pte Ltd. 2019  
K. Murali et al. (eds.), *Proceedings of the Fourth International Conference in Ocean Engineering (ICOE2018)*, Lecture Notes in Civil Engineering 23,  
[https://doi.org/10.1007/978-981-13-3134-3\\_30](https://doi.org/10.1007/978-981-13-3134-3_30)

## 1 Introduction

Fixed offshore platforms have been used for extraction of oil and gas. These platforms were primarily constructed using steel frames made of tubular members welded at joints or specially fabricated joints. The tubular joints and members of the steel structures are subjected to cyclic loading due to wave and wind during its design life. Further, in some cases, the design life may also be extended due to prolonged period of production of oil and gas depending on the availability of oil and gas, which also increases the period of cyclic loading. The tubular joints are vulnerable to fatigue-induced cracks which may propagate during the lifetime. The joint strength capacity reduces as the crack length/depth increase in its size and it eventually fails by brittle fracture or ductile deformation, if repair of the cracks is not carried out on time.

The estimation of residual strength of cracked tubular joints is a subject matter of interest for decades; two methods are widely accepted as approaches relevant and appropriate. The first method is based on reduction factor  $F_{AR}$  applied to the ultimate strength and the reduction factor is calculated based on method described by BS 7910 [1]. The second method is developed based on failure assessment diagram (FAD) as described by BS 7910 [1]. The reduction factor approach focuses only on ultimate strength of cracked tubular joints, whereas the FAD approach focuses on ductile tearing effect of crack.

Earlier investigations have focused on reduction in joint strength for part through thickness cracks in T, DT and K joints under axial tension. This resulted in reduction factor  $F_{AR}$  proposed by Burdkein [2], and subsequently the reduction factor  $F_{AR}$  had undergone further modifications by BS 7910 [1]. The plastic collapse capacity ( $P_{u-c}$ ) of cracked tubular joint is predicted by applying this reduction factor  $F_{AR}$  to ultimate capacity of uncracked tubular joint ( $P_u$ ). In these investigations, the crack locations were arbitrarily chosen at crown or saddle points of weld toe in the tubular joint and which extends up to 33% of perimeter of chord brace intersection. In reality, the crack initiates at the hotspot location of tubular joint and not always at crown or saddle location. There seems to be some degree of variation in the conservativeness of the reduction factor, so a penalty factor has been proposed by Lie et al. [3, 4] for residual static capacity of pre-cracked square hollow section (SHS) joints and tubular joints, respectively.

The difficulties involved in numerical modelling of cracked tubular joints are modelling of weld at tubular joint, crack geometry and crack tip singularity [3, 4]. The T-tubular joints have been considered as specially fabricated joints without welding as stated by Lee [5]. Generally, the cracks are irregular in shape and vary up to any length [6]. In numerical analysis, the crack tip is considered as sharp [6] and a regular crack shape needs to be assumed. In order to capture the effects of crack and crack deformation, appropriate element type and mesh is required [7–9].

There have been extensive studies on element type and mesh techniques to capture crack tip singularity and crack effects. Previously, the programs like PATRAN, NASTRAN, ANSYS, PRETUBE and PMBSHELL were used for mesh generation of cracked tubular joints. Even though automatic mesh generation capabilities are

available, the necessity of an upgraded mesh generation has been addressed by Lie et al. [7–9] to capture crack tip singularity and crack effects. To implement upgraded mesh, improved skill over meshing strategy is required. The crack problems have been solved using virtual crack extension or closure technique [3, 4, 7–9]. The shortcomings of FEM formulation for numerical modelling of crack is overcome by extended finite element method (XFEM) [10–12]. The XFEM technique uses enrichment functions for crack modelling. This enrichment function ensures for crack tip singularity in this analysis. Since XFEM modelling is available in ABAQUS [12] package, this software package was used for the present study. The residual static strength of cracked tubular joints has been estimated using nonlinear XFEM and compared with codal provision of BS 7910 [1].

## 2 Methodology

### 2.1 Numerical Modelling of Uncracked Tubular Joints

A typical cross-sectional view of the T-tubular joint is shown in Fig. 1a. The geometrical dimensions of tubular joints are expressed as non-dimensional parameters, such as diameter ratio  $\beta = d/D$ , thickness ratio  $\tau = t/T$  and chord slenderness ratio  $\gamma = D/2T$ , where  $D$  is the chord diameter,  $d$  is the brace diameter,  $t$  is the thickness of brace and  $T$  is the thickness of chord, respectively. The corresponding non-dimensional parameters used for the simulation are  $\beta = 0.3\text{--}0.9$ ,  $\tau = 0.3, 0.5$  and  $0.7$  and  $\gamma = 10, 20, 30$  and  $40$ . The chord diameter ( $D$ ) of the tubular joint is 750 mm. The chord ends are fixed and the brace end is restrained except in axial direction to allow the axial loads as shown in Fig. 1b. The actual boundary conditions for the chord ends are partially fixed as the ends may rotate due to joint flexibility. In order to avoid short chord effects and stiff joint, the length of chord is assumed as  $L_c = 5D$  and the length of brace was taken as  $L_b = 3d$ . Thus, the non-dimensional chord length parameter  $\alpha = 2L_c/D$  becomes 10, which falls within the applicability range of 4–40 as per API RP 2A [13].

The steel material properties used for the simulation is summarised in Table 1. The material selected is in accordance with the recommendations of API RP 2A [13]. The nonlinear finite element analysis method is based on arc length (RIKS) as proposed in reference [14] which is used in the present study and the solution procedure is available in ABAQUS [12]. This method has been used to determine the ultimate capacity and deformation of tubular joints. The eight-node brick elements are used as it will have facility to simulate through thickness crack. To obtain the hotspot stress around the joint intersection, procedure from DNV-RP-C203 [15] has been adopted, which requires small element sizes around the joints.

In order to reduce the number of elements, coarse mesh was used away from the joint and denser mesh around the joint as suggested by Lee [5] and Lie et al. [7–9].

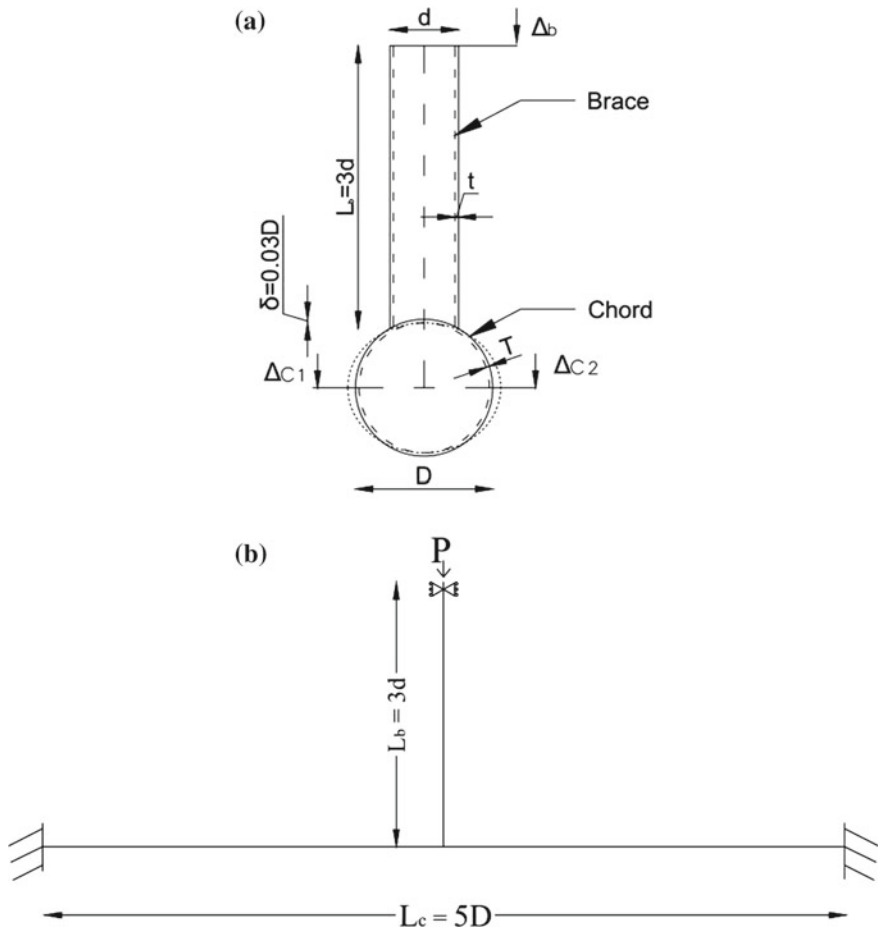


**Fig. 1** a Cross-section view of tubular joints, b boundary conditions of tubular joint

**Table 1** Material properties

$E$ (MPa)	$\mu$	$\sigma_y$ (MPa)	$\sigma_u$ (MPa)	Elongation (%)
$200 \times 10^3$	0.3	240	410	20
$200 \times 10^3$	0.3	345	490	25

The generated mesh is shown in Fig. 2. This varying mesh was surrounded by the same size of elements around the joint which extends up to  $0.8D$  from the centre of intersection in chord and up to  $0.4D$  in brace from the chord surface. The limits used in varying mesh were arbitrary and it was sufficient to cover the length required to obtain SCF. The numerical model proposed in this paper to evaluate the static strength of cracked and uncracked joints has been validated using experimental data

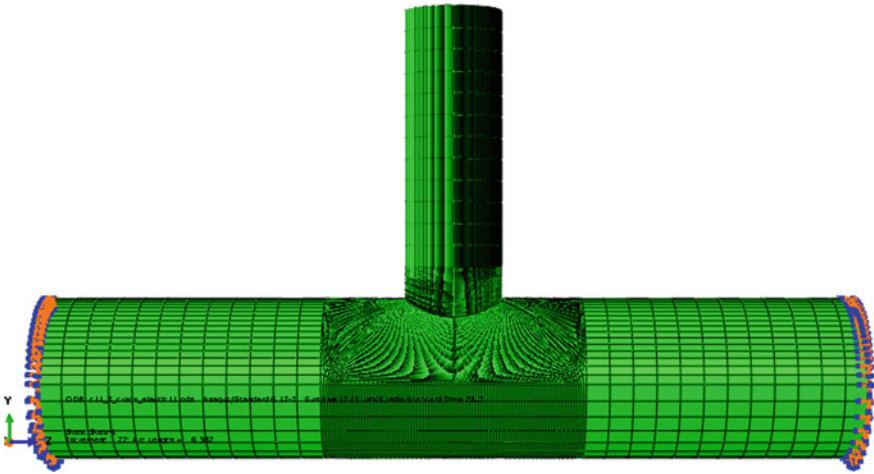


Fig. 2 Meshed geometry of tubular joint with varying element sizes

published in Lie et al. [4] for uncracked tubular joint. Hence, the same numerical modelling technique has been adopted for both uncracked and cracked tubular joints, so that the results can be compared.

## 2.2 Numerical Modelling of Crack in Tubular Joints

The location of pre-crack for simulation has been selected based on the stress concentration factor (SCF) obtained from uncracked tubular joints. The hotspot location was observed in and around saddle position as expected and extends up to 20 mm for  $\beta < 0.6$ . This was due to punching action and ovalizing flexibility of the chord, the brace member transfers most of the load at saddle position. As the diameter ratio ( $\beta \geq 0.6$ ) approaches unity, the brace transfers the load tangentially on to the chord, thus hotspot location can be observed in crown and saddle with slight deviations. This can be substantiated by dramatic increase in the ultimate capacity of joints.

The present study focuses on residual strength of small crack length in hotspot and non-hotspot regions. The crack length used for analysis is summarised in Table 2a, b for part through and through thickness crack. Since the T-tubular joint is symmetry in two planes the crack length was considered up to 25% of brace circumference. As stated earlier, cracks can be modelled in XFEM independent of mesh [10–12]. The in-built level set method automatically generates the position of crack with respect to model when the shell is used for representation of crack. It can also be written in the input file using signed distance ( $\Phi$ ,  $\Psi$ ) value for respective nodes. The signed distance is the distance between the discontinuity (crack) and the nearest nodes. For example, in a 2D mesh layout (see Fig. 3a), the signed distance value shall be (0.5,

**Table 2** a. Part through thickness crack geometry and crack locations. b. Through thickness crack geometry and crack locations

Case	$\beta$	$\gamma$	$2c$ (mm)	$a$ (mm)	Cracked area (mm <sup>2</sup> )	% of crack length = $2c/\pi d$	Crack tip
(a)							
TN12	0.5	20	5	5	19.64	0.4	Crown QP
TN1	0.3	10	5	5	19.64	0.7	Crown
TN5a	0.5	10	13.13	10	103.12	1.1	Saddle
TN8a1	0.8	10	30	18	424.15	1.6	Saddle
TN8a2	0.8	10	30	18	424.15	1.6	Crown
TN4	0.5	10	20	10	187.5	1.7	Crown
TN6a	0.6	10	24	10	188.5	1.7	Crown
TN6a1	0.6	10	30	18	424.15	2.1	Saddle
TN6a2	0.6	10	30	18	424.15	2.1	Crown
TN2a	0.3	10	20	10	157.09	2.8	Saddle
TN3a1	0.4	10	28	18	424.15	3.0	Saddle
TN10a1	0.4	20	30	10	235.62	3.2	Saddle
TN8a3	0.8	10	60	18	848.23	3.2	Saddle
TN8a4	0.8	10	60	18	848.23	3.2	Crown
TN16a	0.3	30	30	7	164.93	4.2	Saddle
TN2a1	0.3	10	30	18	424.15	4.2	Saddle
TN6a3	0.6	10	60	18	848.23	4.2	Saddle
TN6a4	0.6	10	60	18	848.23	4.2	Crown
TN9a1	0.3	20	30	10	235.62	4.2	Saddle
TN8a5	0.8	10	90	18	1272.34	4.8	Saddle
TN8a6	0.8	10	90	18	1272.34	4.8	Crown
TN3a2	0.4	10	54	18	848.23	6.0	Saddle
TN7	0.7	10	100	10	785.4	6.1	Saddle QP
TN10a2	0.4	20	60	10	471.23	6.4	Saddle
TN6a5	0.6	10	90	18	1272.34	6.4	Saddle
TN6a6	0.6	10	90	18	1272.34	6.4	Crown
TN16a2	0.3	30	60	7	326.84	8.5	Saddle
TN2a2	0.3	10	60	18	848.32	8.5	Saddle
TN9a2	0.3	20	60	10	471.23	8.5	Saddle
TN3a3	0.4	10	84	18	1272.34	9.0	Saddle
TN10a3	0.4	20	90	10	766.85	9.5	Saddle
TN16a3	0.3	30	90	7	494.8	12.7	Saddle
TN2a3	0.3	10	90	18	1272.34	12.7	Saddle
TN9a3	0.3	20	90	10	766.85	12.7	Saddle

(continued)

**Table 2** (continued)

Case	$\beta$	$\gamma$	$2a$ (mm)	$b$ (mm)	Cracked area (mm <sup>2</sup> )	% of crack length = $2a/\pi d$	Crack tip
(b)							
TN15	0.9	20	14.2	37.5	532.5	0.7	Saddle
TN8b	0.5	10	20	37.5	750	1.1	Saddle
TN6b	0.6	10	211.5	37.5	7931.3	12.8	Crown QP
TN3b	0.4	10	141.3	37.5	5298.8	15	Crown QP
TN2b	0.3	10	176.5	37.5	6618.5	25	Saddle
TN5b	0.5	10	294.4	37.5	11038.8	25	Saddle QP

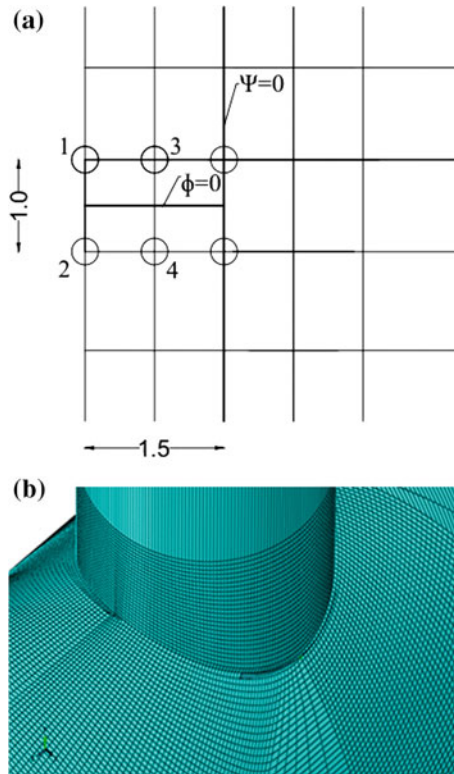


**Fig. 3** **a** Typical 2D Mesh showing nodal distance and crack location, **b** meshed joint with crack pre-set location for XFEM analysis

–1.5) at node 1, similarly it can be written for other nodes. The level set method is to track discontinuity using signed distance function. This was incorporated in XFEM [12] to track the crack tip with respect to nearby nodes. The jump (Heaviside) and asymptotic function [12] are used to capture the discontinuity at prescribed nodes

and crack tip singularities, respectively. These functions are enriched for a radius equal to 3 times the characteristic element length from the crack tip by default [12]. The complexity of crack is limited by the given three-dimensional shell in XFEM. Based on SCF, the crack has been assigned at position using three-dimensional shell, as shown in Fig. 3b. Then, the XFEM method was applied to estimate the residual static strength and predict the failure using J-integral from elastic and elastic-plastic analysis.

### 3 Results and Discussion

#### 3.1 Validation of Numerical Model

The geometric and material properties of joint UT5 used for the validation have been taken from Lie et al. [4] and the same is summarised in Table 3. The validation study has been carried out using varying mesh with finer mesh near the footprint of the brace brick elements. Mesh details and the ultimate capacity obtained from the simulation are summarised in Table 4 and shown in Fig. 4a, b. The sizes of elements were varied from 20 to 1.75 mm. This resulted in total number of elements ranging from 20,000 to 112,290.

The ultimate capacity is defined as the maximum peak load in the load–deformation diagram, i.e. when joint is loaded in compression from brace end which may show a maximum peak load before the load carrying capacity reduces for further deformation. In contrast, there may not be any distinct maximum peak load when joints are subjected to brace end tension. This was evident from the experiment and numerical investigation carried out by Lie et al. [4]. Thus, it is necessary to use

**Table 3** Joint parameters used for validation

Specimen	Brace		Chord		$\sigma_y$ (MPa)	$\sigma_u$ (MPa)	E (MPa)	Elongation
	$d$ (mm)	$t$ (mm)	$D$ (mm)	$T$ (mm)				
UT5	108	6	219	6	290.5	585.8	161.0	25.5%

**Table 4** Summary of ultimate strength of uncracked tubular joint (T5)

Joint ID	Size of element (mm)		No. of elements	Numerical Simulation $P_u$ (kN)			Experiment (Lie et al.) $P_u$ (kN)
	Around joint	Away from joint		$\delta/D =$ 0.03	12.5% $\epsilon$	TES	
UV1	4	20	20,268	197.1	199.2	380	174
UV2	3	20	28,348	196.5	207.4	–	174
UV3	2	20	83,010	204.7	210.0	380	174
UV4	1.75	20	1,12,290	204.7	210.0	380	174

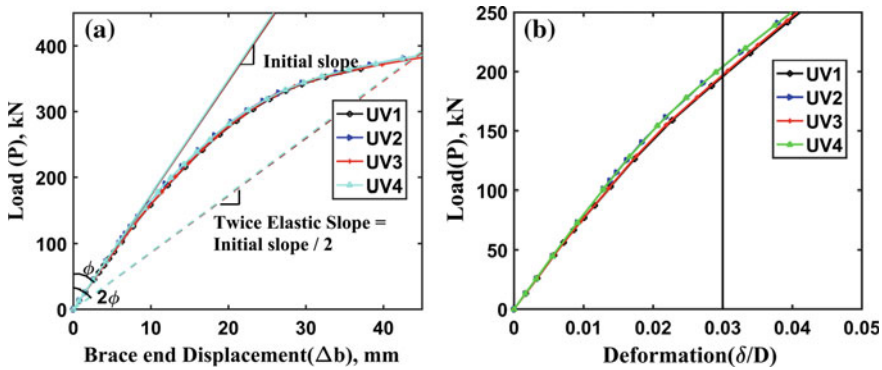


**Fig. 4** a Load (P)—displacement( $\Delta$ ) response, b load (P)—chord deformation ( $\delta/D$ ) response

an appropriate criterion to estimate the ultimate capacity for tensile loaded joints. Several methods exist in literature for the evaluation of ultimate capacity of tubular joints. The noted one commonly used are listed below:

- (a) Twice Elastic Slope (TES) method,
- (b) 12.5% maximum principal strain method,
- (c) 3% chord displacement method.

TES method uses the intersection of a straight line from origin to the load–deflection curve, and the slope of the line is taken as twice the elastic slope ( $\phi$ ) taken clockwise from vertical axis (i.e. load axis). The 12.5% maximum principal strain method uses the load at 12.5% strain as the ultimate capacity. The strain is taken as a peak strain at the chord–brace interface locations. The 3% chord displacement (ovalisation) method uses the load at which the chord displacement becomes 3% of chord diameter.

Lie et al. [4] have used Twice Elastic Slope (TES) criterion to determine the ultimate capacity of tensile loaded joints. The ultimate capacity obtained using this method by Lie et al. [4] for the uncracked tubular joint (UT5) in experiment was 174 kN. The ultimate capacity obtained from numerical simulation by applying TES criteria was 380 kN in all cases, except in one case. Lee and Dexter [16] predicted the ultimate capacity for T- and Y-tubular joints ( $\gamma > 10$ ) using TES. The determined ultimate capacity using TES was widespread when compared with the values obtained from characteristic equations of codal provisions under brace end tension loads. Hence, this method seems to be not recommended for the present investigation of uncracked joints.

The chord ovalisation and first crack were observed by Lee and Dexter [16] on comparing the BOMEL database at an assumed 12.5% maximum principal strain. This criterion was consistent and has some physical significance with ISO characteristic equations. Thus, the 12.5% maximum principal strain criterion has been employed to determine the ultimate capacity in the present study. The ultimate capacity obtained using 12.5% maximum principal strain is varying from 199.2 to 210 kN

for various simulation IDs (UV1, UV2, UV3 and UV4) with different mesh sizes as summarised in Table 4.

The other alternative was to use the serviceability criterion based on chord ovality expressed as  $\delta/D$ . The serviceability criterion of tubular joints [17] was specified as 3% deformation limit of chord wall as shown in Fig. 1a. The 3% chord deformation limit could be obtained by normalising the chord wall displacement ( $\delta$ ) at joint with respect to the diameter of chord ( $D$ ) and excluding chord beam bending due to axial load [16, 17]. This 3% deformation limit is represented in Fig. 4b by drawing solid straight line at ( $\delta/D = 0.03$ ) by excluding chord beam bending. The 3% deformation limit could be used only for uncracked joints as cracks should not occur at serviceability load.

The ultimate capacity estimated using 3% deformation limit varies between 197.1 and 204.7 kN for various cases investigated for the validation study. The brace end displacement ( $\Delta_b$ ) of 12.07 mm is noted at the ultimate capacity as observed from Fig. 4a. The brace displacement ( $\Delta_b$ ) was noted as 21 mm at ultimate capacity from experiments conducted by Lie et al. [5]. The 3% deformation limit (see Fig. 1a) was calculated by subtracting chord beam bending displacement of ( $\Delta_c = \Delta_{c1} + \Delta_{c2}$ ) 5.5 mm. Yura limit [13] was not considered additionally as it was nearby 3% deformation limit. It can be observed from Table 4 that the values estimated using 12.5% strain and 3% chord deformation limit are reasonably closer to that estimated from experiments though the difference between them varies 20% to 16.5%, respectively. However, 12.5% strain limit gave consistent results than the 3% deformation limit, and hence 12.5% strain limit is used in the present study for estimating the ultimate strength of uncracked joints loaded under tension. It is further noted from Table 4 that the mesh convergence has been noted between UV3 and UV4 that the ultimate strength of joint has not changed even though the number of elements has been increased considerably between UV3 and UV4. Hence, the mesh size for all the cases in this study is adopted similar to UV3.

### 3.2 *Ultimate Strength Assessment of Uncracked Tubular Joint*

The ultimate capacity of uncracked T-tubular joints for brace end compression and tension load has been summarised in Table 5 and 6, respectively. The von Mises stress distribution on uncracked tubular joint under tension and compression loading is shown in Fig. 5a, b. The brace punch through was observed for tubular joints loaded under brace end compression as shown in Fig. 5b, whereas the brace pullout was observed for tubular joints loaded under brace end tension as shown in Fig. 5a. The non-dimensional parameter  $Q_u$  has been obtained by dividing the estimated ultimate capacity with yield stress and square of thickness of chord, as shown in Eq. 1. This non-dimensional capacity has been compared with that obtained from

**Table 5** Ultimate capacities of uncracked joints loaded under compression

Joint ID	$\theta$	$\beta$	$\gamma$	$F_y$ (Mpa)	Peak load (kN)	$\delta/D = 0.03$ (kN)	FE $Q_u = P_u/F_y * T^2$	API $Q_u$	FE/API
TN2	90	0.3	10	240	2810	2810	8.33	6.88	1.21
TN3	90	0.4	10	240	3895	3882	11.50	9.26	1.24
TN5	90	0.5	10	240	5076	4921	14.58	12.04	1.21
TN6	90	0.6	10	240	6649	6392	18.94	15.16	1.25
TN7	90	0.7	10	240	7602	7435	22.03	18.62	1.18
TN8	90	0.8	10	240	8848	8599	25.48	22.41	1.14
TN9	90	0.3	20	240	993.4	820.4	9.47	8.13	1.16
TN10	90	0.4	20	240	1210	1140	13.16	11.06	1.19
TN11	90	0.5	20	240	1620	1536	17.73	18.61	0.95
TN13	90	0.6	20	240	2088	2015	23.26	23.02	1.01
TN14	90	0.8	20	240	3065	3064	35.36	33.04	1.07
TN16	90	0.3	30	345	780	581.4	10.79	8.04	1.34
TN17	90	0.5	30	345	926	909	17.18	14.67	1.17
TN18	90	0.6	30	345	1110	1097	20.59	18.69	1.10
TN19	90	0.8	30	345	2021	1684	37.49	33.22	1.13
TN20	90	0.3	40	345	215	210	6.91	8.04	0.86
TN21	90	0.5	40	345	524	496	16.34	14.67	1.11
TN22	90	0.6	40	345	667	658	21.67	18.69	1.16
TN23	90	0.8	40	345	1096	1080	35.58	33.22	1.07
Mean									1.12
Standard deviation									0.14
CoV (%)									12.80

empirical equations based on recommendations of API RP 2A for tubular joints. The non-dimensional capacity for axial load can be expressed as

$$Q_u = \frac{P_u \sin \theta}{F_y T^2} \quad (1)$$

where  $P_u$  is the estimated ultimate capacity of joint against the axial load.

The ultimate simulated capacities ( $P_u$ ) of joints loaded under compression were determined using 3% chord displacement in order to limit the deformation. Moreover, the ultimate capacities estimated using 3% chord displacement limit were similar to maximum peak load, except in few cases. The effect of thickness ratio ( $\tau$ ) on ultimate strength was less as expected, for a common chord slenderness ratio ( $\gamma$ ) and diameter ratio ( $\beta$ ), as shown in Fig. 6a. The non-dimensionalised load–deformation response for compression loaded joints is shown in Fig. 6b, which are typical for other compression loaded joints.

**Table 6** Ultimate capacities of uncracked joints loaded under tension

Joint ID	$\theta$	$\beta$	$\gamma$	$F_y$ (Mpa)	$\delta/D =$ 0.03 (kN)	12.5% $\epsilon$ load (kN)	TES	FE $Q_u$ $= P_u/F_y$ $* T^2$	API $Q_u$	FE/API
TN2	90	0.3	10	240	3095	3052	2900	9.04	9	1.00
TN3	90	0.4	10	240	4158	4075	3880	12.07	12	1.01
TN5	90	0.5	10	240	5291	5100	4800	15.11	15	1.01
TN6	90	0.6	10	240	6370	6200	6100	18.37	18	1.02
TN7	90	0.7	10	240	7398	7185	6980	21.29	21	1.01
TN8	90	0.8	10	240	8496	8247	8100	24.44	24	1.02
TN9	90	0.3	20	345	2070	1563	1968	12.55	9	1.39
TN10	90	0.4	20	345	3140	2597	2980	16.50	12	1.38
TN13	90	0.6	20	345	3930	3488	4272	28.01	18	1.56
TN14	90	0.7	20	240	3348	2700	3000	31.16	21	1.48
TN16	90	0.3	30	345	1080	780	1520	14.48	9	1.61
TN17	90	0.5	30	345	1845	1579	–	29.29	15	1.95
TN18	90	0.6	30	345	1910	1900	1954	35.25	18	1.96
TN19	90	0.8	30	345	3660	2190	3770	40.63	24	1.69
TN20	90	0.3	40	345	728	300	680	9.84	9	1.09
TN21	90	0.5	40	345	1228	750	–	27.88	15	1.64
TN22	90	0.6	40	345	1450	1080	–	35.43	18	1.97
TN23	90	0.8	40	345	2412	1300	2596	42.65	24	1.78
Mean										1.41
Standard deviation										0.37
CoV (%)										25.9

The variation of  $Q_u$  with thickness ratio obtained from simulation has been compared with that estimated using API RP 2A [13] as shown Fig. 6a for  $\gamma = 10$  and 20. The simulated/estimated codal API RP 2A [13] ultimate capacity statistics has been summarised in Table 5, which show a mean of 1.12 and coefficient of variation of 12.8% for T-joints loaded under compression. This indicates overall good correlation between simulated and predicted results. Thus, ultimate capacities are safely underpredicted by the empirical equations of API RP 2A [13] for joints loaded under compression.

As stated earlier, there is no distinct peak for joints loaded in tension which is shown in Figs. 7a, b. The load–deformation response for the  $\tau = 0.5$  and  $\gamma = 10$  joints is shown in Fig. 7a, which is typical for other tension loaded joints. In this plot, the applied load has not been non-dimensionalised in order to compare with TES and 3% chord displacement limit. So, the relative proximity of all the failure criteria can be compared. The residual  $\gamma$  effects are overpredicted after non-dimensionalisation of ultimate capacities as shown in Fig. 7b. The ultimate simulated capacities for joints loaded under tension were determined using 12.5% maximum principal strain criteria. The simulated/codal API RP 2A [13] ultimate capacity statistics has been

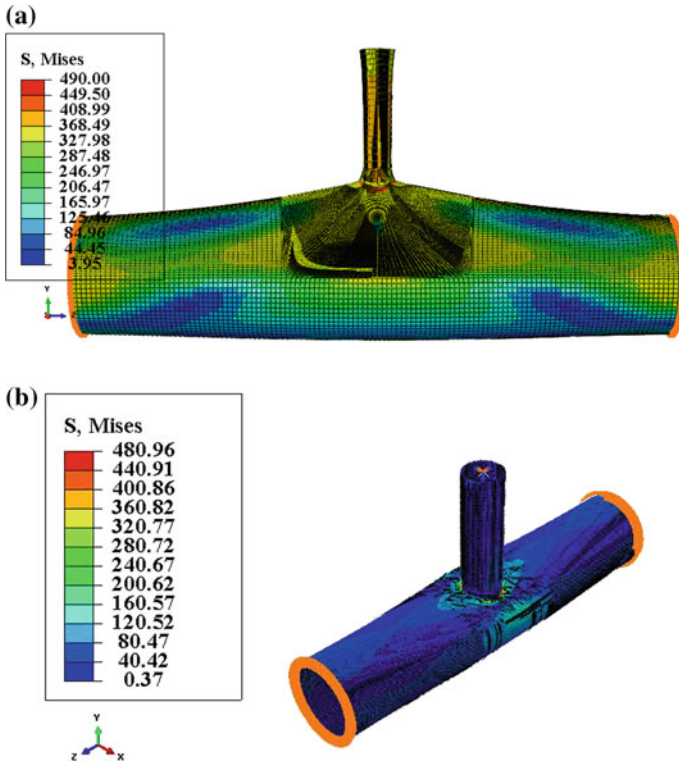


**Fig. 5** **a** Stress distribution of tubular joint under tensile load, **b** stress distribution of tubular joint under compressive load

summarised in Table 6, show a mean of 1.41 and coefficient of variation of 27% for T-joints under tensile loading. This indicates that the ultimate capacities are safely much underpredicted by the empirical equations of API RP 2A [13] for joints loaded under tension.

### 3.3 Residual Strength Assessment of Cracked Tubular Joint

The 12.5% maximum principal strain is a first crack failure criterion [16]. According to serviceability criteria (3% deformation limit), there should be no visible crack in the tubular joints [17]. As the joints are pre-cracked, the criteria such as 12.5% principal strain and 3% deformation limit are not considered for the residual capacity of cracked tubular joints. Hence, the residual strength for cracked tubular joint was estimated using twice elastic slope criterion. This criterion is well established for residual strength of cracked tubular joints [3, 4, 18]. Figure 8a, b represent the

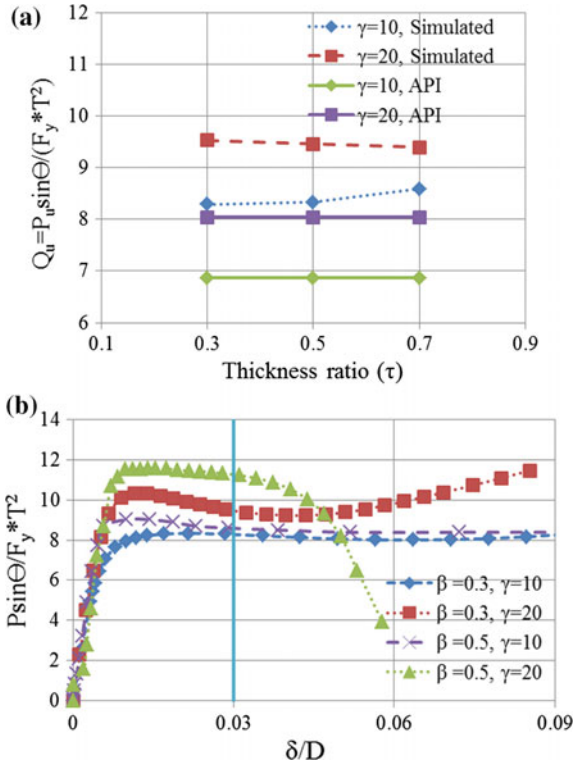


**Fig. 6** a Comparison of FE results for compression loaded joints ( $\beta=0.3$ ) with API, b load–deformation responses for compression loaded joints ( $\tau=0.5$ )

typical deformation of part through thickness crack and through thickness crack, respectively. From the plots Fig. 9a, b, it can be inferred that the initial stiffness slope of cracked remains the same with respect to uncracked tubular joints.

The residual strength of cracked tubular joint can be estimated by applying the reduction factor  $F_{AR}$  to the respective characteristic strength of uncracked tubular joint. The  $F_{AR}$  used for evaluation is as per BS 7910 [1], which is shown in Eq. 2.

$$Reduction\ factor\ F_{AR} = \left( 1 - \frac{A_c}{T * l_w} \right) \left( \frac{1}{Q_\beta} \right)^{mq} \tag{2}$$

$$Q_\beta = 1 \text{ for } \beta \leq 0.6$$

$$Q_\beta = \frac{0.3}{\beta(1 - 0.833)} \text{ for } \beta > 0.6$$

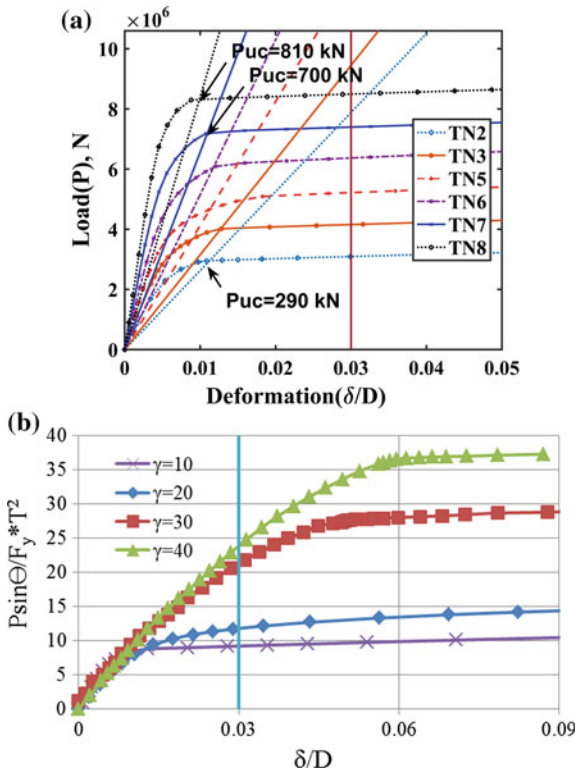


**Fig. 7** **a** Load (P)–deformation ( $\delta$ ) responses for tension loaded joints ( $\tau=0.5, \gamma=10$ ), **b** load (P)–deformation ( $\delta$ ) responses for tension loaded joints ( $\tau=0.5, \beta=0.3$ )

where  $A_c$  = area of crack,  $A_c = 0.5\pi ac$  and  $2ab$  for part through thickness crack and through thickness, respectively,  $l_w = 2\pi rK_a$  as per AWS [19],  $r$  = effective radius of intersection,  $K_a = 1$  for axial load,  $mq = 0$  for part through thickness crack.  $mq = 1$  and  $0$  as per HSE characteristic design strength and API RP 2A [13] design tension strength for through thickness crack.

The non-dimensional parameter ( $Q_{uc}$ ) is obtained in similar as of Eq. (1), expect the ultimate capacity ( $P_u$ ) that is replaced by ( $P_{u-c}$ ). Then, the actual  $F_{AR}$  is obtained by dividing  $Q_{uc}/Q_u$ . The residual strength estimated using BS 7910 [1] method based on  $F_{AR}$  compares reasonably well with that obtained from present numerical simulations as shown in Table 7a. A maximum decrease in estimated residual static strength of cracked is observed to be 8.1% when compared to corresponding ultimate strength of uncracked, in case of TN6a. The residual strength of TN3a was only 0.625 times of TN6a, even though the crack length of TN3a was 10 times of TN6a. This shows that the influence of crack length is not much in the reduction of residual strength.

The reduction in residual strength is significant for joints with smaller diameter ratio ( $\beta$ ) which can be seen in Fig. 10. The residual strength for joints with small

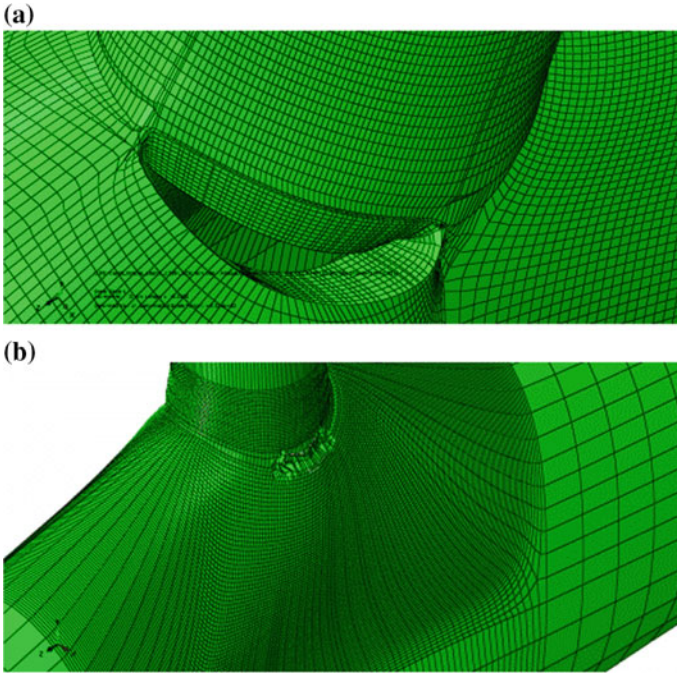


Fig. 8 a Deformation of through, b deformation of part through thickness crack

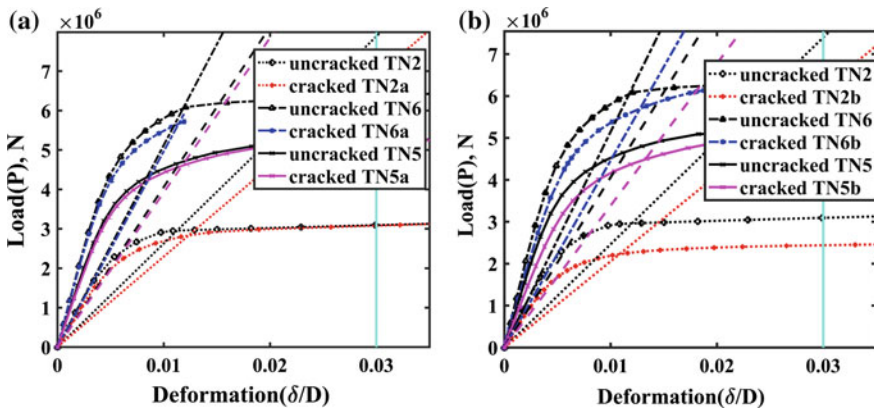
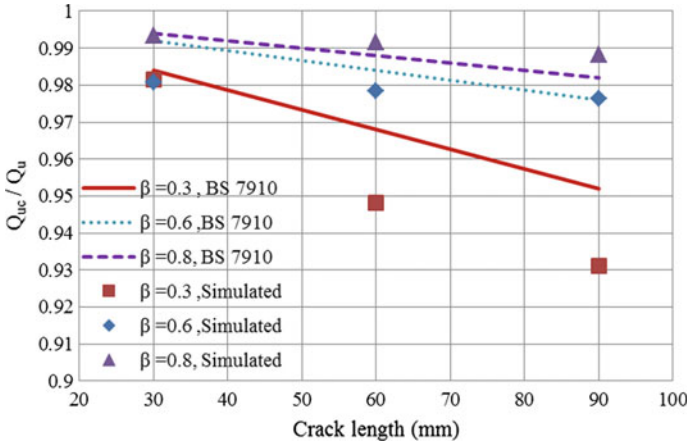


Fig. 9 a Load–deformation response through thickness crack, b load–deformation for response for part through thickness crack

**Table 7** a. Residual strength of joints with part through thickness crack under tension. b. Residual strength of joints with through thickness crack under tension

Case	$P_u$ (kN) {1}	$F_{AR}$ {2}	$P_{c-p}$ (kN) = $\frac{P_u \times F_{AR}}{\{3\}} =$ $\{1\} * \{2\}$	$P_{u-c}$ (kN) {4}	Actual $F_{AR}$ $(\frac{Q_{uc}}{Q_u})$ {4}/{1}	$P_{u-c}/P_{c-p}$ {4}/{3}
(a)						
TN12	1272	0.999	1266.0	1269.0	0.998	1.002
TN1	1980	0.999	1998.5	1978.0	0.999	0.990
TN5a	4800	0.998	4788.8	4790.0	0.998	1.000
TN6a	6100	0.996	6167.7	5600.0	0.918	0.908
TN4	5046	0.996	5028.0	5030.0	0.997	1.000
TN2a	2970	0.994	2952.2	2800.0	0.943	0.948
TN7	7282	0.987	7189.6	7100.0	0.975	0.988
TN3a	4036	0.969	3827.1	3820.0	0.946	0.998
TN2a1	3052	0.984	3003.2	2995.2	0.981	0.997
TN2a2	3052	0.968	2954.3	2894.1	0.948	0.980
TN2a3	3052	0.952	2905.5	2841.5	0.931	0.978
TN3a1	4075	0.989	4030.2	3964.9	0.973	0.984
TN3a2	4075	0.977	3981.3	3915.3	0.961	0.983
TN3a3	4075	0.966	3936.5	3904.3	0.958	0.992
TN6a1	6100	0.992	6051.2	5983	0.981	0.989
TN6a3	6100	0.984	6002.4	5969	0.979	0.994
TN6a5	6100	0.976	5953.6	5955	0.976	1.000
TN6a2	6100	0.992	6051.2	5963	0.977	0.984
TN6a4	6100	0.984	6002.4	5952	0.975	0.990
TN6a6	6100	0.976	5953.6	5992	0.982	1.006
TN8a1	12,000	0.994	11928.0	11,920	0.993	0.999
TN8a3	12,000	0.988	11856.0	11,900	0.992	1.004
TN8a5	12,000	0.982	11784.0	11,860	0.988	1.006
TN8a2	12,000	0.994	11928.0	11,915	0.993	0.998
TN8a4	12,000	0.988	11856.0	11,900	0.992	1.004
TN8a6	12,000	0.982	11784.0	11,885	0.990	1.008
TN9a1	1563	0.982	1534.9	1475.0	0.944	0.961
TN9a2	1563	0.964	1506.7	1445.0	0.925	0.959
TN9a3	1563	0.947	1480.2	1425.0	0.912	0.963
T16a1	780	0.981	765.2	704.8	0.904	0.921
T16a2	780	0.963	751.1	693.3	0.889	0.923
T16a3	780	0.944	736.3	686.1	0.880	0.932
Mean						0.963
CoV (%)						0.93
(b)						
TN5b	4800	0.750	3600.0	4539	0.945	1.260
TN6b	6090	0.858	5314.3	5762	0.931	1.100
TN2b	2970	0.750	2227.5	2210	0.744	0.992
TN3b	4036	0.850	3430.9	3785	0.938	1.080
TN8b	8363	0.989	8112.9	8248	0.986	1.017
Mean						1.090
CoV (%)						9.63



**Fig. 10** Comparison of reduction in strength with crack length at saddle location for different diameter ratios  $\beta$  and  $\gamma=10$ ,  $\tau=0.5$

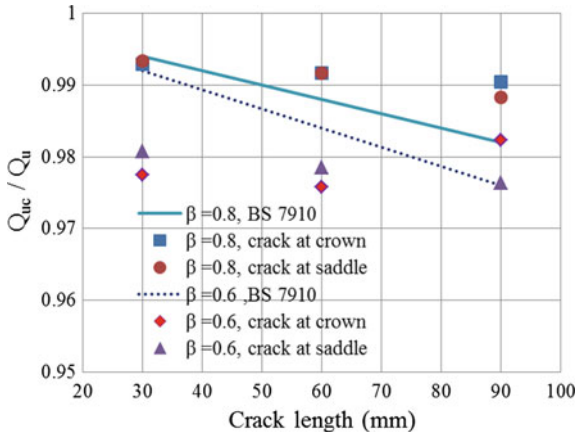


**Fig. 11** Comparison of reduction in strength with crack length for different crack locations and  $\gamma=10$ ,  $\tau=0.5$

diameter ratio ( $\beta=0.3, 0.4$ ) decreased by an average of 1.3% in addition to the existing reduction factor ( $F_{AR}$ ). The residual strength is higher for the same crack length present on increasing diameter ratio. The reduction in residual strength is of similar manner irrespective of hotspot position, i.e. crown or saddle at higher diameter ratio ( $\beta>0.6$ ), which can be seen from Fig. 11.

The residual strength decreases on increasing the chord slenderness ratio for a common crack length and diameter ratio, which can be seen in Fig. 12. The residual strength for joints with increasing chord slenderness ratio  $\gamma=10-30$  decreased by an average 3% in addition to the existing reduction factor ( $F_{AR}$ ). It is known that the

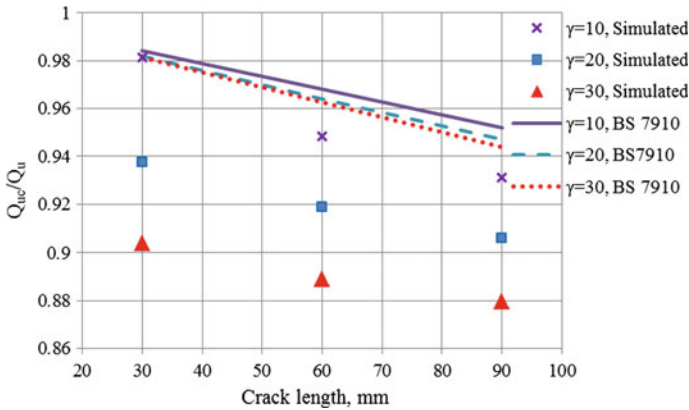


**Fig. 12** Comparison of reduction in strength with crack length at saddle location for different chord slenderness ratios  $\gamma$  and  $\beta = 0.3$ ,  $\tau = 0.5$

reduction factor as per BS 7910 [1] is based on  $\beta$ ,  $T$  and  $l_w$ . In general, the strength of joint reduces as the chord slenderness ratio increases. So, this chord slenderness factor needs to be considered.

The residual strength of joints with through thickness crack loaded under tension has been summarised in Table 7b. The maximum reduction in strength for through thickness crack was 26%, in case of TN2b. This shows that the joint has residual capacity even when the crack length was 25% of brace circumference.

The reduction in residual strength varies based on crack type which can be seen on comparing cases TN5a (part through thickness crack) and TN8b (through thickness crack). These two joints have crack tip at hotspot (saddle) and the same percentage of crack length (1.1%). The reduction in strength is higher for TN8b ( $\beta = 0.8$ ) compared to TN5a ( $\beta = 0.5$ ), even though  $\beta$  is higher compared to TN5a. This shows that through thickness crack results in higher reduction of residual strength.

The residual static strength for brace end compression load cases is summarised in Table 8a, b for part through and through thickness crack, respectively. The reduction in residual static strength was less irrespective of crack type, under brace end compression load which can be noted from Table 8a, b. The influence of brace end loading on residual strength has been examined under both load cases. It has been noticed that reduction in residual strength was higher in case of brace end tensile load rather than compressive load which can be seen in cases of TN1 and TN2a. Thus, an overall reduction of 5% was estimated in addition to the existing reduction factor as per BS 7910 [1] for joints with part through thickness crack loaded under tension. The reduction factor as per BS 7910 [1] was satisfactory for through thickness crack under tension loading.

**Table 8** a. Residual strength of joints with part through thickness crack under compression. b. Residual strength of joints with through thickness crack under compression

Case	$P_u$ (kN) d{1}	$F_{AR}$ {2}	$P_{c-p}$ (kN) $= P_u \times F_{AR}$ {3}={1}*{2}	$P_{u-c}$ (kN) {4}	$P_{u-c} / P_{c-p}$ {4}/{3}	Actual $F_{AR}$ ( $Q_{uc} / Q_u$ ) {4}/{1}
(a)						
TN1	1971	0.999	1969.0	1962	0.996	0.995
TN2a	2977	0.994	2959.5	2957	0.999	0.993
(b)						
TN15	3353	0.990	3319.2	3293	0.992	0.982

## 4 Summary and Conclusion

### 4.1 Summary

The FE simulations were carried out for uncracked and cracked T-tubular joints under axial compressive and tensile loading. On comparing, the simulated ultimate capacities of uncracked tubular joints with codal provisions (API RP 2A [13]), a good correlation was obtained, even though there are some deviations due to  $\gamma$  effect. This demonstrates the validity of numerical procedure.

The hotspot location was observed in and around saddle position as expected and extends up to 20 mm for  $\beta < 0.6$ . As the diameter ratio ( $\beta \geq 0.6$ ) approaches unity, the hotspot location can be observed in crown and saddle with slight deviations. The residual strength was obtained using twice elastic slope criterion for cracked tubular joints.

### 4.2 Conclusion

The residual strength depends upon crack location, crack type, crack shape, load applied and also geometric parameters of tubular joints such as  $\beta$  and  $\gamma$  ratio. From simulations, the following were observed:

- If the crack is present at the saddle location (hotspot), the reduction in residual strength is higher at smaller diameter ratio  $\beta < 0.6$  compared to  $\beta \geq 0.6$ .
- The reduction in residual strength is in similar manner irrespective of hotspot location, i.e. crown or saddle, when  $\beta \geq 0.6$ .
- In the existing reduction factor (BS 7910 [1]) an additional 5% deduction is suggested, while estimating the residual strength, for part through thickness crack in tubular joints ( $\beta \leq 0.6$ ,  $\gamma > 10$ ) loaded under tension.
- The existing reduction factor (BS 7910 [1]) is conservative for through thickness crack in tubular joints loaded under tension.

- The through thickness crack results in much reduction of strength compared to part through thickness crack. The joint has residual capacity even when the crack length was up to 25% of brace circumference.
- The residual strength reduction was less for tubular joints under compression loading as expected.

The residual strength has been obtained by considering tubular joints as specially fabricated. A weld correction factor is needed to be used in order to employ these residual strengths to tubular joints with weld.

## References

1. British Standards 7910 (2005) Guide to methods for assessing the acceptability of flaws in metallic structures, vol 3
2. Burdekin FM (2001) The static strength of cracked joints in tubular members. Offshore technology report OTO-2001/080, Healthy and Safety Executive, London, UK
3. Lie ST, Li T, Shao YB (2017) Fatigue and fracture strength of a multi-planar circular hollow section TT-joint. 129:101–110. <https://doi.org/10.1016/j.jcsr.2016.11.001>
4. Lie ST, Li T, Shao YB (2014) Plastic collapse load prediction and failure assessment diagram analysis of cracked circular hollow section T-joint and Y-joint. *Fatigue Fract Mater Struct* 314–324. <https://doi.org/10.1111/ffe.12115>
5. Lee MMK (1999) Strength of ring-stiffened tubular T-joints in offshore structures—a numerical parametric study. 51:239–264
6. Anderson TL (1995) *Fracture mechanics*. CRC press
7. Lie ST, Lee CK, Chiew SP, Shao YB (2005) Mesh modelling and analysis of cracked uni-planar tubular K-joints. *J Constr Steel Res* 61:235–264. <https://doi.org/10.1016/j.jcsr.2004.05.006>
8. Lie ST, Lee CK, Wong SM (2003) Model and mesh generation of cracked tubular Y-joints 70:161–184
9. Lie S, Lee C, Chiew S (2006) Static strength of cracked square hollow section T joints under axial loads II: numerical. *J Struc Eng* 132:378–386
10. Dolbow J, Belytschko T (1996) A finite element method for crack growth without remeshing. *Int J Numer Methods Eng* 46(1):131–150
11. Jitpaired K (2015) Fatigue behavior and xfem based life prediction of tubular x-joints with concrete filled chord. PhD thesis submitted to National University of Singapore
12. ABAQUS (2012) ABAQUS theory manual, Version 6.12. Hibbitt, Karlsson and Sorensen Inc, Pawtucket, Rhode Island
13. American Petroleum Institute (2014) Recommended practice for planning, designing and constructing fixed offshore platforms—working stress design
14. Riks E (1979) An incremental approach to the solution of buckling and snapping problems. *Int J Solids Struct* 15:524–551
15. Det NorskeVeritas (2011) Recommended practice—C203. Fatigue design of offshore steel structures
16. Lee MMK, Dexter EM (2004) Finite element modelling of multi-planar offshore tubular joints. *ASME* 126:120–128
17. Wardenier J Hollow sections in structural applications. *Comite International pour la' Developpement et Etude de la construction tubulaire*

18. Taliie-Faz B, Dover WD, Brenan FP (2000) Static strength of cracked high strength steel tubular joints. *Health and Safety Executive* 78:1–53
19. American Welding Society (2006) D.1.1.-1 Structural welding code—steel